IOPscience iopscience.iop.org

Home Search Collections Journals About Contact us My IOPscience

A structural study on a-GaP prepared at different temperatures

This article has been downloaded from IOPscience. Please scroll down to see the full text article.

1992 J. Phys.: Condens. Matter 4 7759

(http://iopscience.iop.org/0953-8984/4/38/009)

View the table of contents for this issue, or go to the journal homepage for more

Download details:
IP Address: 171.66.16.96
The article was downloaded on 11/05/2010 at 00:35

Please note that terms and conditions apply.

J. Phys.: Condens. Matter 4 (1992) 7759–7772. Printed in the UK

A structural study on a-GaP prepared at different temperatures

N Elgun, S J Gurman and E A Davis
Department of Physics and Astronomy, University of Leicester, Leicester, UK

Received 14 April 1992, in final form 25 June 1992

Abstract. A series of nearly stoichiometric a-GaP films has been prepared by RF sputtering on to substrates held at temperatures from 20–200 °C. Extended x-ray fine absorption (EXAFS) at both the Ga and P K edges, infrared absorption, and optical edge data have been used to understand the structures of these films. The stoichiometric amorphous network of GaP, which was found to be fourfold coordinated as expected, showed no chemical disorder. The development of the atomic order of the network with increasing deposition temperature and annealing, from the amorphous to the crystalline state, has been followed. The results are discussed in terms of the bond lengths and angles and the strength of the Ga–P bonds.

1. Introduction

Crystalline III–V semiconductors are important materials owing to their technological applications in the microelectronic and optoelectronic industries. Their amorphous counterparts have become of interest recently, not only because of their possibility for applications, but also because of their contribution to fundamental research on non-crystalline systems.

The structural disorder in the amorphous materials is the basic factor that determines their properties and can be categorized as being either chemical or configurational. Configurational disorder refers to the variations in bond lengths and angles, which affect the localization of the states at the band edges and the band gap. Chemical disorder relates to the proportion of each type of chemical bond present and influences the electronic valence and conduction band densities of states and, as for configurational disorder, the size of the band gap. In contrast to amorphous group-IV elements which have only configurational-type disorder, amorphous III–V compounds, being binaries, can also contain chemical disorder. This has been investigated for amorphous GaAs [1, 2, 3], GaP [4] and InP [5] by EXAFS. In the case of a-GaAs, since the shape of the scattering factors for both Ga and As atom are nearly identical, it is very difficult to draw conclusions about chemical disorder. However, in the case of a-GaP the scattering factors of Ga and P atoms are very different so that EXAFS becomes a more sensitive test of chemical disorder. Chemical disorder in flash-evaporated a-GaP has already been reported [6].

Only a few IR studies on a-GaP [7, 8] and a-GaP:H [9, 10] have so far been made. In one of these [7] IR spectra have been obtained from 6 to 300 K. In the present work, the change in the IR absorption bands of a-GaP with increasing deposition

0953-8984/92/387759+14$04.50 © 1992 IOP Publishing Ltd

temperature and on annealing (up to 673 K) have been investigated and the results compared with c-GaP.

The aim of the present work is to investigate the structure of sputtered amorphous GaP films using EXAFS and infrared techniques.

2. Sample preparation

The films used for both EXAFS, infrared analysis and optical measurements were prepared by RF sputtering at the same time so as to eliminate deposition-dependent variations. The base pressure before flushing argon into the chamber was 2×10^{-7} mTorr, and the pressure during sputtering was 3–4 mTorr. The power applied to the 4″ stoichiometric polycrystalline GaP target was 250 W. For infrared and optical measurements, polished crystalline silicon wafers and fused-silica substrates respectively were used. The distance between the target and substrates was kept at 5 cm. For EXAFS measurements on the P edge, the films were deposited on to Cu plates because of the need to have a conductive substrate required for the drain current measurement, whereas for the Ga edge, mylar was used as a substrate, the films being folded over many times until the optimal thickness 40–50 μm was obtained for the x-ray transmission measurements made at this edge.

Films were deposited on substrates held between room temperature and 200 °C. (These films will be referred to as a-GaP(T_s) where T_s is the deposition temperature.) Some samples prepared at room temperature were subsequently held at higher temperatures (200–400 °C) for two hours at a base pressure of 10^{-5} mTorr in order to investigate the structure of annealed samples. (These films will be referred to as a-GaP(T_a) where T_a is the annealing temperature.)

The deposition rates were between 30 and 40 Å min^{-1} depending on the deposition temperature. The thicknesses of the films (1–1.2 μm) were determined both by an optical technique, in which the interference fringes in reflection were used, and by a mechanical method using a Taysurf. The thicknesses determined by both methods agreed to within 5%.

The compositions of the samples were determined by both energy-dispersive x-ray analysis (EDAX) using a DS 130 scanning electron microscope (SEM) and EXAFS in which the step heights of the absorption spectra taken at the P K edge were used. Both methods were consistent with one another. The compositions of the films were found to fluctuate around stoichiometry within 2–4%. The uniformity of the composition across the films was also checked by taking line profiles for both Ga and P in EDAX. The line profiles showed that for some films the P content, but not the Ga content, varies somewhat across their width. A few per cent argon was found to be trapped in the films.

The amorphicity of the samples was checked both by a JOEL Jem 100Cx transmission electron microscope, from which characteristic diffuse-ring diffraction patterns were obtained, and by the EXAFS technique itself. The transmission electron microscope was also used to look at the surfaces of the films in order to probe any phase separation. Within the resolution of the microscope, the surfaces of all samples were smooth and showed no phase separation except one prepared at 200 °C whose surface was slightly rough and displayed features which we associated with regions where an excess of P exists.

3. Experimental details and data analysis

3.1. EXAFS

The x-ray absorption spectra of samples for both the Ga and P K edges were obtained using the 2 GeV Synchrotron Radiation Source at the SERC Daresbury Laboratory.

The Ga K edge experiments in the nearly hard-x-ray region (~ 10 370 eV) were carried out at the 7.1 beam line station in the transmission mode at room temperature. In the beam line, the white x-ray beam is collimated at the entrance slit, monochromatized using a Si(111) crystal with harmonic rejection set at 70%, and passed through the folded sample whose thickness, d, was about 40–50 μm. Both the incident I_0 and transmitted beam intensity I were measured by ion chambers filled with argon gas. The x-ray absorption spectra were obtained by comparing the transmission beam intensity to the incident beam intensity as the energy region was scanned.

The P K edge experiments in the soft-x-ray region (~ 2150 eV) were made at room temperature at the 3.4 beam line station where the electron drain current method, which is a modification of the total electron yield technique, is used. At station 3.4, the white beam is monochromatized using a Ge(111) crystal and focused on the sample by a chromium-coated mirror placed at a grazing angle. Because of the strong attenuation of such low-energy x-rays by the atmosphere, the mirror, the monochromator and the samples have to be maintained in ultra-high vacuum. The absorption of x-ray photons by the sample causes electron ejection. As a result, a drain current, which is proportional to the absorption coefficient $\mu(E)$, can be collected and measured.

The EXAFS function, $\chi(E)$, was obtained from the absorption spectrums $\mu(E)$ by making pre- and post-edge background subtractions using the available software program, EXBACK. For both of these subtractions, different-order polynomials have been fitted. The normalized EXAFS function $\chi(E)$, was first converted into $\chi(k)$ using

$$\hbar^2 k^2/2m = (E - E_{\text{edge}}) + E_0$$

where E is the incident photon energy, E_{edge} is the threshold energy of that particular absorption edge and E_0 is the energy offset, being the difference between the energy of a $k = 0$ photoelectron and the lowest unoccupied energy level. $\chi(k)$ is then multiplied by k^3 in order to compensate for the diminishing amplitudes of the experimental spectrum at high k-values. In order to obtain structural information, the program EXCURV90 was used to make a comparison of the least-squares fitting of the k^3-weighted experimental spectrum to the theoretical spectrum which was calculated using the single-scattering curved wave theory [11]. The basic formula describing the theoretical EXAFS spectra is

$$\chi(k) = (-A(k)/k) \sum_j (N_j/R_j^2)|f_j(k)| \exp(-2\sigma_j^2 k^2) \\ \times \exp(-2R_j/\lambda) \sin(2kR_j + 2\delta + \psi).$$

Here $f_j(k)$ is the backscattering amplitude from each of the N_j neighbouring atoms of the jth type, with a Debye–Waller factor of σ_j^2, at a distance R_j away. δ is the phaseshift experienced by the photoelectron during its passage through the

central-atom potential, and ψ is the phase of the backscattering factor. The term $\exp(-2R_j/\lambda)$ is due to inelastic losses in the scattering process with λ being the electron mean free path. λ can be written in terms of a constant imaginary part of the potential, VPI, as $\lambda = k/\text{VPI}$. $A(k)$ is the amplitude reduction factor due to many-body effects such as shake-up and shake-off processes at the central atom [12]. During the fitting, the values used for both $A(k)$ and VPI were 0.75 and −5 at the Ga and 0.65 and −3.5 at the P K edges respectively, which were the result of the least-squares fitting for crystalline GaP, and the phaseshifts of both the absorbing and neighbouring atoms were calculated in the program. The least-squares refinements of the experimental and theoretical spectra were terminated when the least-squares fit index was minimized. The fit index, FI, is defined by

$$\text{FI} = (1/100N_\text{p})\sum_i\{[\chi_i(\text{calc}) - \chi_i(\text{exp})]k^n\}^2$$

where N_p is the number of data points in the spectrum, and n is a k-weighting factor, which was kept at 3 throughout this work. The uncertainty in the final set of parameters resulting from such a procedure has been found as pairs of $(N_j,\ \sigma_j^2)$ and $(R_j,\ E_0)$ by using a statistical test described by Joyner *et al* [13]. In the test, the error bars of the paired fitting parameters are given by the 95% confidence region $(\pm 2\sigma)$ of a contour map of the fit index.

In the present work, in addition to the extraction of the conventional structural information, EXAFS has been used to find the compositions of the samples. For this purpose, only the absorption spectrum of the P K edge can be used, because the drain current is then obtained from the first 100 Å or so below the sample surface, containing no contribution from the substrate. Therefore, the relative step height of $\mu(E)$ can be written as the sum of the atomic absorption of each element. For $Ga_{1-x}P_x$,

$$\mu(E) = (1-x)\mu_\text{Ga} + x\mu_\text{P}.$$

By taking the ratio of values of $\mu(E)$ just above and just below the edge and the atomic absorption coefficients given by [14], the compositions x were calculated.

The absorption edge itself and the spectrum $\sim$ 25 eV above it had to be excluded from the EXAFS function since the theory used for EXAFS takes into account only the single-scattering process, whereas in the region close to the edge multiple-scattering processes are dominant. However, this region (called the XANES region) was used to obtain information on the partial conduction band density of states.

3.2. *Infrared spectroscopy*

Infrared spectra of the samples in the frequency range 4000–200 cm^{-1} were obtained at room temperatures by using a Model 580B double-beam Perkin–Elmer infrared spectrophotometer. A c-Si wafer was used in the path of reference beam in order to eliminate the effect of substrates. Also during the scans, dry air was flushed into the sample compartment to remove water vapour which causes extra absorption bands and complicates the spectra.

3.3. *The optical measurements*

The reflection and transmission of the films in the UV/visible/near-infrared region were measured at room temperature using a Model 330 Perkin–Elmer spectrophotometer. Assuming that the films are weakly absorbing, the absorption coefficients, α, of the films were calculated from the following formula

$$T = (1 - R)\exp(-\alpha t)$$

where T and R are the measured transmittance and reflectance, respectively, and t is the film thickness.

4. Results and discussion

Figures 1 and 2 show the k^3-weighted EXAFS function χ and Fourier transform for crystalline and amorphous GaP at the Ga and P K edges. It is not surprising that all the fine structure of the EXAFS function of the crystalline state has disappeared in the EXAFS functions of the amorphous state. Similarly, while the Fourier transforms of the EXAFS from the crystal show strong features up to the third shell, only the first-shell peak is strong in the amorphous case. This is expected in the absence of periodicity and can be used as a test of amorphicity.

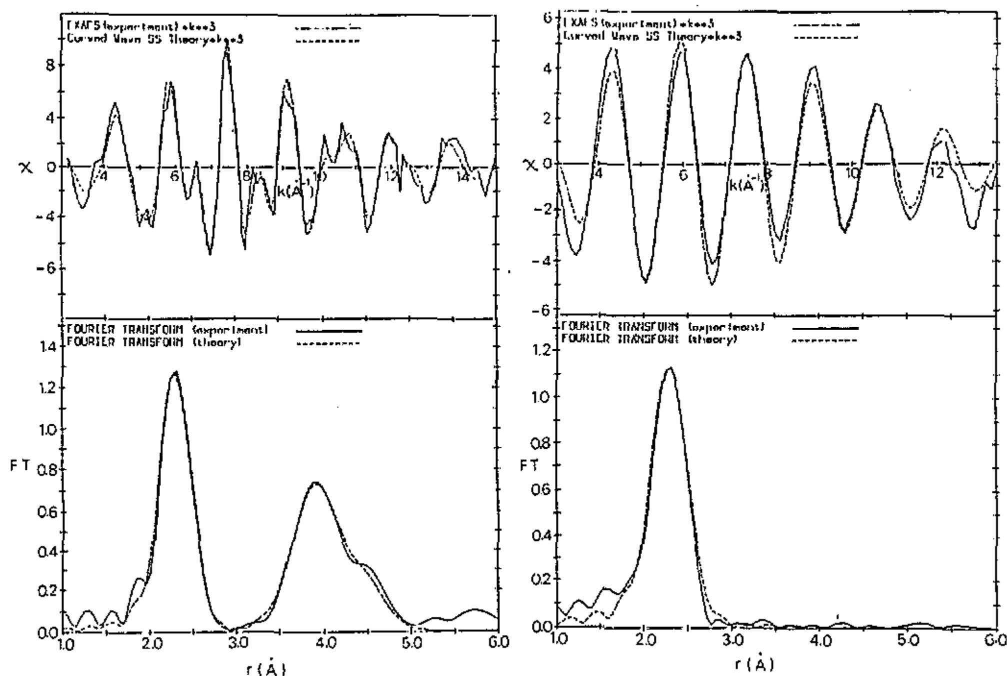

Figure 1. The k^3-weighted EXAFS function χ and Fourier transform FT for crystalline (on the left) and amorphous (on the right) GaP ($T_s = 20$ °C) at the Ga K edge.

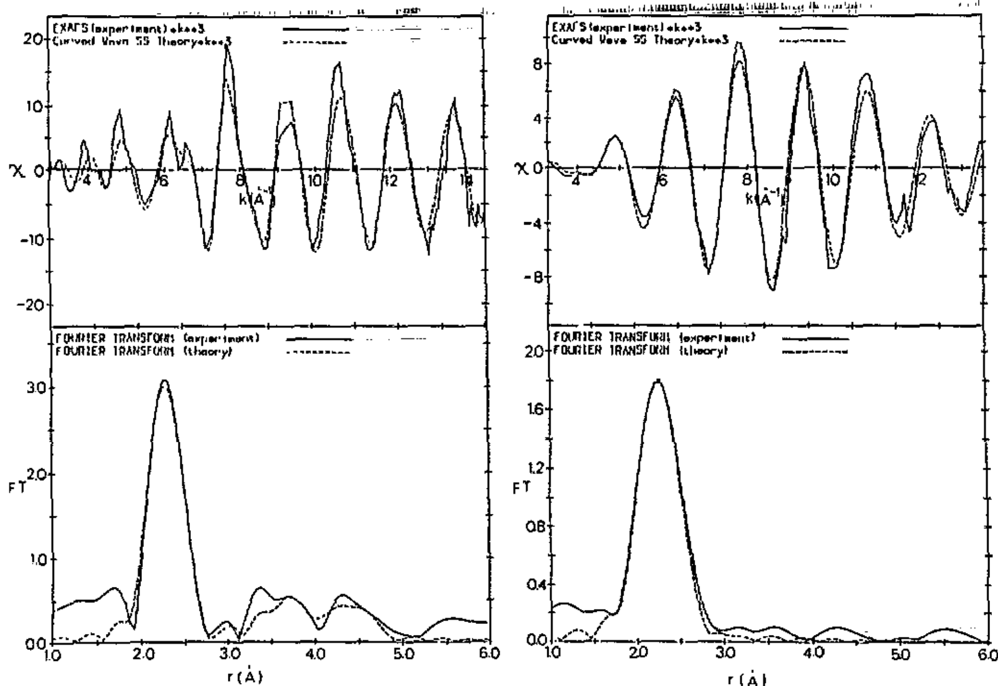

Figure 2. The k^3-weighted EXAFS function χ and Fourier transform FT for crystalline (on the left) and amorphous (on the right) GaP (T_s = 20 °C) at the P K edge.

The EXAFS data in the k-range 3–13.5 Å^{-1} for both the P and Ga edges of the samples prepared at high deposition temperatures T_s and also of the samples annealed at temperatures T_a, have been analysed as described in section 3.1. During the data analysis not only Ga–P bonds but also P–P and Ga–Ga bonds were added into the fitting process. However, in every case, the program EXCURV90 rejected the existence of the P–P and Ga–Ga bonds, which shows that wrong bonds are not found in the structure of the samples on a significant scale. (The sensitivity of EXAFS is such that the existence of bonds down to 5% can be detected with the large data range used.) The coordination numbers, the length of the Ga–P bond and the spread of the bond lengths (the so-called Debye–Waller factor) have been determined, and are shown in figures 3, 4 and 5, respectively. Figure 3 confirms that a-GaP is fourfold coordinated; in other words, it consists of tetrahedral units. This structure is maintained at higher deposition and annealing temperatures. The Ga–P bond length is also independent of the T_s and T_a temperatures as can be seen from figure 4. The values we found for the Ga–P bond lengths lie around 2.33 and 2.31 Å in the case of a-GaP, and 2.33 and 2.325 Å in the case of c-GaP, the two values corresponding to data taken at the Ga and P edges, respectively. Our crystalline bond length is about 0.03 Å less than the value extracted from diffraction experiments [15]; we believe that this arises from a slight difference in the phaseshift used. However, because the same phaseshift is used for all amorphous samples as well as the crystal, this discrepancy does not affect any of the conclusions made here. In any case there is a 0.02 Å difference in the nearest-neighbour distance determined using the two edges, which is probably within the experimental errors. However, comparison of the amorphous bond length with that of the crystal using the two edges is important since it forms the basis of our

discussion concerning the existence or otherwise of chemical order on a small scale in this amorphous III–V compound. If a-GaP is chemically disordered, we should detect P–P bonds (2.2 Å) at the P edge and Ga–Ga bonds (2.44 Å) at the Ga edge, in addition to the bonds between Ga and P atoms. Therefore, we would expect to see an increase in the measured Ga–P bond length at the Ga edge and a decrease in the measured P–Ga bond length at the P edge compared to the bond lengths in the crystal, since EXAFS gives an average value for bond lengths. However, we could see only a 0.015 Å difference between the crystalline and amorphous bond lengths at the P edge, which is well below the experimental error of 0.03 Å, and no difference at all at the Ga edge. Thus, we conclude from the bond length data that a-GaP is chemically ordered.

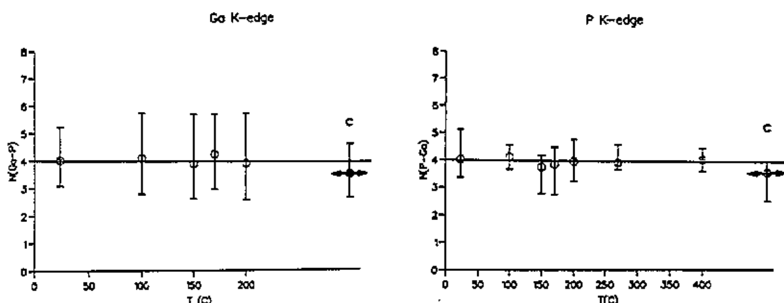

Figure 3. Coordination numbers determined at the Ga and P K edges versus deposition or annealing temperatures. The points marked with c and an arrow are for c-GaP and added into the figure for comparison.

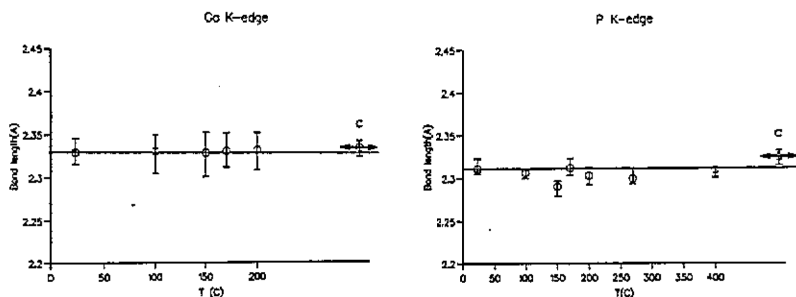

Figure 4. Lengths of the Ga–P bond determined at the Ga and P K edges versus deposition or annealing temperatures. The points marked with c and an arrow are for c-GaP and added into the figure for comparison.

The question of chemical order or disorder can also be discussed using the bond-conservation criterion

$$c_i N_{ij} = c_j N_{ji}$$

where $c_{i,j}$ are the compositions of the type of atoms i, j forming a bond and N_{ij} is the number of j atoms bonded to an i atom. The criterion has been applied to a-GaP by using the coordination numbers determined from EXAFS and the composition

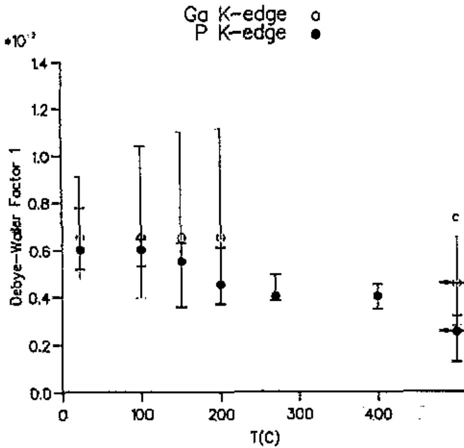

Figure 5. Debye–Waller factor of the first shell as a function of deposition or annealing temperature for the Ga and P K edges. The points marked with c and an arrow are for c-GaP and added into the figure for comparison. All data were taken at room temperature.

values obtained from EDAX. It was found that the above equation is satisfied within the experimental error. Therefore, again we conclude that a-GaP is chemically ordered.

Infrared spectroscopy can provide information on both the nature and the number of bonds of each type and hence can be used to investigate the existence, if any, of wrong bonds. The transmission spectra of a-GaP at high wavenumbers shows structure associated with the interference fringes. Therefore, only the range 1000–200 cm^{-1} is shown in figure 6(*a*) in which the main feature is due to the stretching mode of the Ga–P bond. Wrong bonds, i.e. P–P and Ga–Ga, are infrared inactive in the crystalline state. However, because the selection rules are relaxed in the amorphous state owing to the lack of periodicity, all modes can contribute to the spectra. Thus, wrong bonds, if present, should be seen in the IR spectrum. If we had P–P bonds in our a-GaP samples, we would have expected to see structure [16] at ~ 270, ~ 360 and ~ 450 cm^{-1}, or, at least, at one of these wavenumbers. None of these features was seen and hence, we conclude that a-GaP contains no P–P bonds (or at least less than 10% of the total bonds, which is the detectable limit of the IR spectroscopy), i.e. it is chemically ordered.

The disorder in the network of the a-GaP films has been changed gradually from the amorphous to the crystalline state by increasing the deposition and annealing temperature. Changes can be seen in the Debye–Waller factors of the first and second shell given in figures 5 and 7 for data obtained from both edges. As can be seen from figure 5, the values determined for the Debye–Waller factors of the first shell, σ_1^2, at the Ga and P edges are consistent with one another. This is expected since they both show the spread of the same bond length, namely the Ga–P bond, and thus we have a consistency check on the fitted values. The values of σ_1^2 decrease with increasing deposition and annealing temperature and approach the crystalline values, indicating a reduction in the configurational (static) disorder of the bond length. The result is also consistent with the optical data in figure 8, where the optical band gap is seen to increase with the increasing deposition temperature from the amorphous band gap value towards that of the crystal. Figure 7 also shows that the variations of the next-nearest-neighbour distances at both edges, i.e. the Ga–Ga distance on the Ga edge and P–P distance on the P edge, are different. The effect of this result on the structure is important and will be discussed in terms of bond angles below.

For amorphous materials, the Debye–Waller factor determined experimentally has

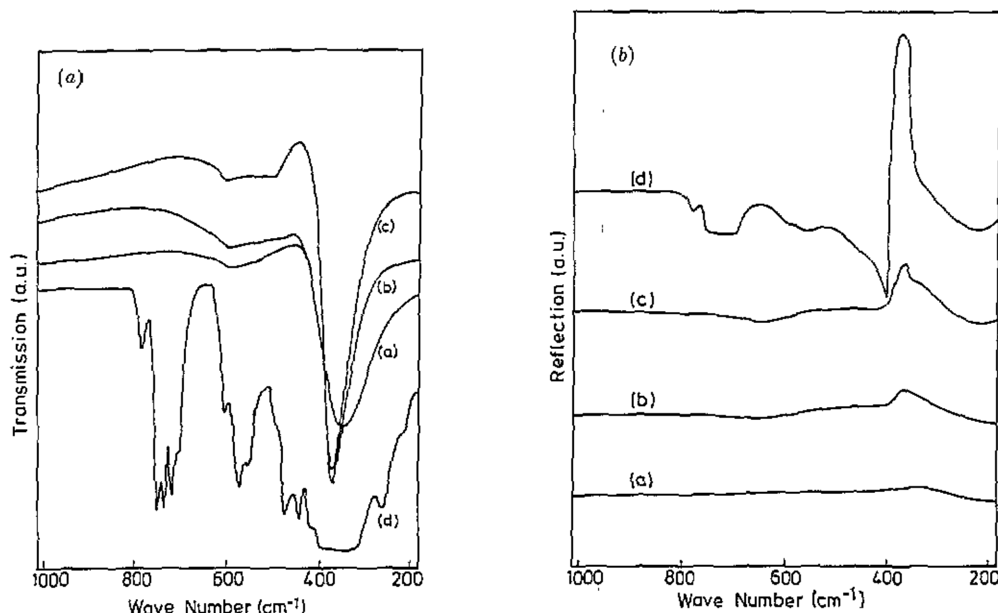

Figure 6. (*a*) Transmission spectra of (a) a-GaP (T_s = 20 °C), TO mode at 345 cm^{-1}; (b) a-GaP (T_s = 200 °C); (c) a-GaP (T_a = 400 °C), TO mode at 370 cm^{-1} for (b) and (c); (d) c-GaP, three-phonon process at 784 cm^{-1}, TO + TO at 750 cm^{-1}, LO + TO at 735 cm^{-1}, LO + LO at 720 cm^{-1}, TO + TA at 572 cm^{-1}, LO + LA at 555 cm^{-1}, TO + TA_1 at 492 cm^{-1}, LO + TA_1 at 475 cm^{-1}, TO + TA_2 at 442 cm^{-1}, LO + TA_2 at 425 cm^{-1}. The errors in the quoted wavenumbers are a few cm^{-1}. (*b*) Reflection spectra of (a) a-GaP (T_s = 20 °C); (b) a-GaP (T_s = 200 °C); (c) a-GaP (T_a = 400 °C); (d) c-GaP; the TO mode at 370 cm^{-1} is consistent with (*a*).

contributions from both thermal and static disorder

$$\sigma^2(\exp) = \sigma^2_{\text{thermal}} + \sigma^2_{\text{static}}.$$

Assuming that there is no static disorder in the crystalline state, the above equation becomes $\sigma^2_{\text{thermal}} = \sigma^2_{\text{cry}}(\exp)$. Then the static disorder of the amorphous materials can be easily determined. Using the values of the Debye–Waller factor of the first shell, both $\sigma^2_{\text{thermal}}$ and σ^2_{static} of a-GaP were found to be about 0.003 Å^2. This much static disorder causes a 0.007 Å change in the bond length of 2.33 Å. This means that the length of the Ga–P bond in the amorphous state is hardly different from the length of the same bond in the crystal, a feature which is true for many amorphous materials. The fact that we still have an amorphous structure suggests a wide spread in bond angles. In the present work, we have attempted to find the mean value of the bond angle as well as its spread. Figures 9(*a*) and (*b*) show three tetrahedra units joined to each other in 3D and a small part of its top view in 2D, respectively. By using the nearest-neighbour distance (2.33 Å) and the next-nearest-neighbour distances (3.8 Å for both Ga–Ga and P–P distances), the mean value of the bond angle β has been determined as 109.3°, which is the bond angle in the crystalline state. When the spread in the bond angle was being calculated from the Debye–Waller factor of the second shell, σ_2^2, however, it was found necessary to introduce two different spreads around the same mean value, $\Delta\beta_1$ and $\Delta\beta_2$, due to the differences in the values of the Debye–Waller factors of the second shell at the

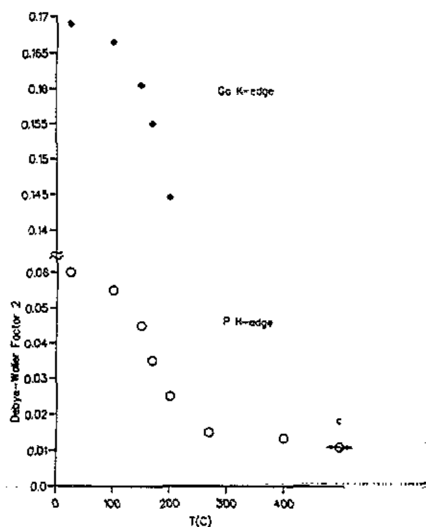

Figure 7. Debye–Waller factors of the second shell as a function of deposition or annealing temperature for the Ga and P K edges. The points marked with c and an arrow are for c-GaP and added into the figure for comparison. All data were taken at room temperature.

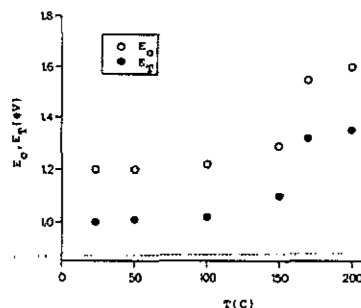

Figure 8. Optical gaps as a function of deposition temperature. E_0 is the photon energy where $\alpha = 10^4\ \mathrm{cm}^{-1}$, whereas E_T is the Tauc gap.

Ga and P edges. In the calculation of $\Delta\beta_1$ and $\Delta\beta_2$, the contribution of thermal disorder of the second shell ($\sigma^2_{\text{thermal}} = 0.011$ Å^2) has been subtracted from the experimental Debye–Waller factor as has been done for the first shell, and thus the static bond-angle spreads were obtained. The values of the static bond angle spreads shown in table 1 should be compared to the thermal bond-angle spread which is 1.2° for all samples. It was found that the angle $\beta_2 = \beta \pm \Delta\beta_2$ varies more than the angle $\beta_1 = \beta \pm \Delta\beta_1$, and both angle spreads decrease with increasing deposition and annealing temperature. This result shows that the bond angle at Ga is more rigid than that at P.

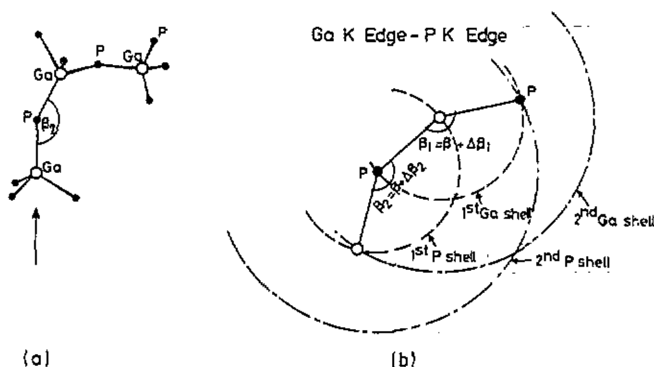

Figure 9. (a) Three GaP tetrahedra units in 3D. (b) Top view of a small part of (a) in 2D together with radii of the first and second shells associated with the Ga and P K edges.

Table 1. The static bond angle spreads, $\Delta\beta_1$ at the Ga edge and $\Delta\beta_2$ at the P edge, in samples with different deposition, T_s, and annealing, T_a, temperatures. The temperature T refers to either T_s or T_a. ($\beta_1 = \beta \pm \Delta\beta_1$, $\beta_2 = \beta \pm \Delta\beta_2$.)

T (°C)	20	100	150	170	200	270	400
$\Delta\beta_1$	5.4	4.8	3.7	2.6	1.5	0.4	0.3
$\Delta\beta_2$	17.3	17.0	16.3	15.7	14.6	—	—

Infrared spectroscopy can again be used to follow the development of the order in the network. Figures 6(a) and (b) compare the transmission and reflection spectra of a-GaP(T_s = 20 °C), a-GaP(T_s = 200 °C) and a-GaP(T_a = 400 °C) with each other as well as with c-GaP. The observed bands in c-GaP have been assigned to different modes using published assignments [17], (see figure 6(a)). In the case of the amorphous samples, most of the fine structure seen in the IR spectra of c-GaP has been smeared out either partially or completely, but, with increasing deposition and annealing temperature, the TO mode becomes sharper and shifts to higher wavenumber and more structure gradually starts appearing at 500 and 600 cm^{-1} in the IR transmission spectra. Similarly, the IR reflection spectra start showing more structure around 650 cm^{-1} and the reflection coefficient at 370 cm^{-1} increases. The shift of the fundamental stretching mode from 345 to 370 cm^{-1}, which is known as the fundamental stretching frequency of c-GaP, can be associated with the increase in bond strength. Using the simple harmonic oscillator approach, the force constant k, which is a measure of bond strength, was calculated for the wavenumbers before and after the shift. It was found that k increased by 15% after the shift, meaning that the Ga–P bonds are becoming stronger with increasing order in the network. As is known, c-GaP has the zincblende structure in which the s and p orbitals hybridize as sp^3 in order to maximize the bond energy and to make the bonds as strong as possible. In the case of a-GaP, the sp^3 hybridization is somewhat different from that of c-GaP, resulting in less strong bonds. This is presumably due to the variations in the bond angle.

A XANES spectrum which is the part of the x-ray absorption spectrum close to the absorption edge actually represents the density of states of the conduction band. XANES is, therefore, complementary to the techniques such as x-ray emission or x-ray and UV photoelectron spectroscopy (XPS and UPS) which give information on the density of states of the valence band.

Figures 10(a) and (b) show the XANES of P and Ga K edges for both amorphous and crystalline samples, i.e. the partial density of states of the conduction band for each type of atom. The first striking thing about these figures is that there is a lot of smearing of the features present in the XANES of c-GaP in the amorphous case. The first peaks which occur at 10 364 and 2144 eV for Ga and P edges, respectively, are associated with the antibonding p-like bands since they correspond to 1s → p transitions. The second and third peaks at the P edge, which become more pronounced with increasing temperature, correspond to the antibonding mixed s–p and s-like bands, respectively. However, the latter two peaks seen in the crystalline case at the Ga edge do not recover with temperature up to 200 °C.

In figure 11, the XANES spectra of both crystalline and amorphous GaP at the P edge (d), (e) are plotted together with the K_β x-ray emission spectrum [18] of P in c-GaP (a), XPS [19] of c-GaP (b) and UPS [20] of a-GaP ($h\nu = 21.2$ eV) (c). From

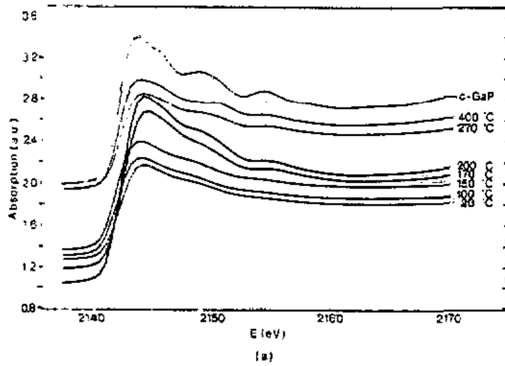

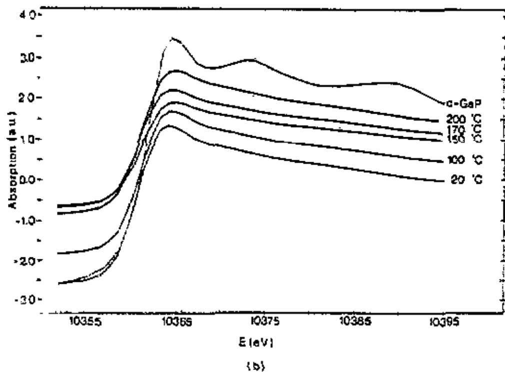

Figure 10. XANES for (*a*) The P K edge (*b*) The Ga K edge. The curves have been displaced for clarity.

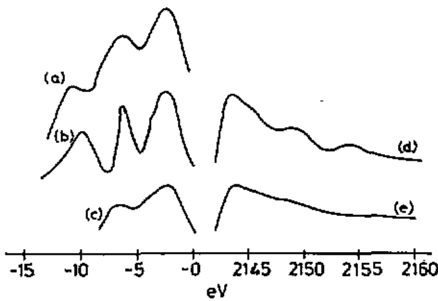

Figure 11. (a) K_β x-ray emission spectrum [19] of P in c-GaP; (b) XPS [20] of c-GaP; (c) UPS [21] of a-GaP ($h\nu = 21.2$ eV); (d) XANES of c-GaP at the P K edge; (e) XANES of a-GaP at the P K edge.

a comparison of these spectra (an allowance should be made amongst the spectra because of the different techniques used), we firstly note that the density of states of the valence (a), (b) and the conduction bands (d) of c-GaP are mirror images of one another as expected from a bonding-antibonding picture. However, a comparison of the density of states of the valence band (c) with the conduction band (e) of a-GaP prepared at room temperature shows that, while the valence band has fewer features than that of the crystal, the conduction band loses its structure nearly completely. The same result has been found for a-Ge and a-Si [21]. Secondly, the density of states of the conduction bands for both amorphous and crystalline samples are broadened

compared to the density of states of the valence bands due to transitions from the deep-lying d levels of Ga (binding energy = −18.7 eV [19]) to the conduction band [22].

5. Conclusions

In this paper, we have presented a detailed structural study of nearly stoichiometric sputtered a-GaP films prepared at a temperature range of 20–200 °C and annealed up to 400 °C. The local structure and bonding of these films have been investigated by using EXAFS at both the Ga and P K edges and infrared spectroscopy. The results were also correlated with optical edge data.

In the amorphous network of GaP, Ga and P atoms are found to be tetrahedrally coordinated, as expected. The existence of wrong bonds, i.e. Ga–Ga and P–P bonds, in the structure has been discussed and it is concluded that a-GaP contains no (or very few, below the detectable limits of the techniques used) wrong bonds, i.e. it is chemically ordered.

It was also found that there is no appreciable disorder in the bond length but there are very wide spreads in the bond angles due to the amorphous nature of these films. The bond angle spread at P in particular is much larger than that at Ga which shows that a P-centred tetrahedron is not as rigid as a Ga-centred tetrahedron. The disorder in the network of the films has been changed gradually from the amorphous to the crystalline state by increasing the deposition and annealing temperatures. There are no changes in the coordination numbers and in the Ga–P bond length with increasing deposition and annealing temperature but there is a decrease in the bond angle spread, an increase in the optical band gap and an increase in the strength of the Ga–P bond.

Finally, our XANES spectra have been combined with the XPS, UPS and K_β x-ray emission spectra taken from the literature so that a complete picture of the electronic valence and conduction band densities of states of the a-GaP films can be obtained.

Acknowledgments

The authors would like to thank Dr A Singh and Dr S H Baker for useful discussions and T Foxon from the Philips Research Labs for supplying the sample of c-GaP.

References

[1] Del Cueto J A and Shevchik N J 1978 *J. Phys. C: Solid State Phys.* **11** L829
[2] Theye M L, Gheorghiu A and Launois H 1980 *J. Phys. C: Solid State Phys.* **13** 6569
[3] Baker S H, Manssor M I, Gurman S J, Bayliss S C and Davis E A 1992 *J. Non-Cryst. Solids* **144** 63
[4] Udron D, Flank A M, Gheorghiu A, Lagarde P and Theye M L 1989 *Phil. Mag. Lett.* **59** 9
[5] Flank A M, Lagarde P, Udron D, Fission S, Gheorghiu A and Theye M L 1987 *J. Non-Cryst. Solids* **97–8** 435
[6] Udron D, Flank A M, Gheorghiu A, Lagarde P and Theye M L 1989 *Physica* B **158** 625
[7] Prettl W, Shevchik N J and Cardona M 1973 *Phys. Status Solidi* b **59** 241
[8] Buckel W J and Lakshmi G 1975 *Phys. Status Solidi* b **70** K113
[9] Wang Z P, Ley L and Cardona M 1983 *Physica* B **117–18** 968
[10] Ghosh B K and Agrawal B K 1986 *J. Phys. C: Solid State Phys.* **19** 7157

[11] Gurman S J, Binsted N and Ross I 1984 *J. Phys. C: Solid State Phys.* **17** 143
[12] Azaroff L V 1974 *X-Ray Spectroscopy* (New York: McGraw-Hill) section 5
[13] Joyner R W, Martin K J and Meehan P 1987 *J. Phys. C: Solid State Phys.* **20** 4005
[14] Viegele W J 1973 *At. Data* **5** 51
[15] Harrison W A 1980 *Electronic Structure and the Properties of Solids* (San Francisco, CA: Freeman)
[16] Extance P 1981 *PhD Thesis* University of Cambridge
[17] Willardson R K and Beer A C (ed) 1967 *Semiconductors and Semimetals* vol 3 (New York: Academic)
[18] Wiech G 1968 *Z. Phys.* **216** 472
[19] Ley L, Pollak R A, McFeely F R, Kowalczyk S P and Shirley D A 1974 *Phys. Rev.* B **9** 600
[20] Shevchik N J, Tejeda J and Cardona M 1974 *Phys. Rev.* B **9** 2627
[21] Mott N F and Davis E A 1979 *Electronic Processes in Non-Crystalline Materials* (Oxford: Clarendon)
[22] Grobman W D, Eastman D E and Freeouf J L 1975 *Phys. Rev.* B **12** 4405